Microfluidics and Nanofluidics (2018) 22:48
https://doi.org/10.1007/s10404-018-2067-z

RESEARCH PAPER

Solving lubrication problems at the nanometer scale

Nisha Chandramoorthy[1] · **Nicolas G. Hadjiconstantinou**[1]

Received: 24 September 2017 / Accepted: 4 April 2018

Abstract
Lubrication problems at lengthscales for which the traditional Navier–Stokes description fails can be solved using a modified Reynolds lubrication equation that is based on the following two observations: first, classical Reynolds equation failure at small lengthscales is a result of the failure of the Poiseuille flowrate closure (the Reynolds equation is derived from a statement of mass conservation, which is valid at all scales); second, averaging across the film thickness eliminates the need for a constitutive relation providing spatial resolution of flow profiles in this direction. In other words, the constitutive information required to extend the classical Reynolds lubrication equation to small lengthscales is limited to knowledge of the flowrate as a function of the gap height, which is significantly less complex than a general constitutive relation, and can be obtained by experiments and/or offline molecular simulations of pressure-driven flow under fully developed conditions. The proposed methodology, which is an extension of the generalized lubrication equation of Fukui and Kaneko to dense fluids, is demonstrated and validated via comparison to molecular dynamics simulations of a model lubrication problem.

1 Introduction

Molecular dynamics (MD) simulation (Allen and Tildesley 1989; Frenkel and Smit 2002) has been a valuable asset in the study of nanoscale fluid mechanics and transport, finding extensive use by researchers studying a variety of nanoscale problems, ranging from flows around and through carbon-based nanostructured materials (Mattia et al. 2015; Guo et al. 2015; Secchi et al. 2016; Popadić et al. 2014) to boundary lubrication problems (Zheng et al. 2013; Berro et al. 2010; Savio et al. 2013). In some cases, the systems of interest are sufficiently small, that a direct simulation is feasible (Berro et al. 2010; Zheng et al. 2005). In other cases, when direct simulation is not possible, MD has been used to provide insight into the physics of these flows (Landman et al. 1996; Priezjev et al. 2005).

However, despite the insight gained on a number of aspects of nanoscale flow by MD studies, a general description of such flows beyond Navier–Stokes has yet to be developed for dense fluids. In fact, in many instances, different studies reach contradictory conclusions (Ghorbanian et al. 2016), with the only clear consensus being that the Navier–Stokes description remains remarkably robust, at least up to scales as small as $O(10\ \text{nm})$. This can be qualitatively explained by noting that, for a dense fluid, the characteristic fluid lengthscale, $\hat{\sigma}$, is on the order of the molecular size; deviations from Navier–Stokes, expected as the characteristic flow lengthscale becomes smaller than $O(10\ \hat{\sigma})$ (Travis et al. 1997; Sofos et al. 2009; Ghorbanian and Beskok 2016), should therefore manifest themselves at lengthscales of $O(1\text{–}10\ \text{nm})$, depending on the fluid. A similar argument correctly predicts Navier–Stokes breakdown in rarefied gases to occur at much larger, $O(\mu\text{m})$, scales (Hadjiconstantinou 2006), owing to the significantly larger size of the mean free path compared to the molecular size.

The present paper focuses on a particular class of problems, namely of the lubrication type, for which progress can be made using the following observation, originally due to Fukui and Kaneko (1988): in lubrication problems, averaging across the film thickness (made possible by the small film thickness) eliminates the need for spatial resolution of flow profiles in the transverse film direction. In other words, knowledge of the flowrate due to the local pressure gradient is sufficient for closing the governing (lubrication) equation, thus reformulating the problem from one of finding the general constitutive relation for the stress tensor to that of finding the *fully developed* flowrate in response to

✉ Nicolas G. Hadjiconstantinou
ngh@mit.edu

Nisha Chandramoorthy
nishac@mit.edu

[1] Department of Mechanical Engineering, Massachusetts Institute of Technology, Cambridge, MA 02139, USA

Published online: 11 April 2018

a pressure gradient. The importance of this simplification cannot be overstated: lubrication theory (Leal 2007; Szeri 2011) separates the effects of axial variations (captured by the lubrication equation) from the constitutive relation (for the flowrate), allowing the latter to be determined once and for all in the significantly simpler, lower-dimensional setting of the fully developed flow (with no axial variation).

As stated above, this approach has already been exploited by Fukui and Kaneko (1988) who have developed a "generalized lubrication equation" (GLE) for treating dilute gas lubrication problems. In their case, they used solutions of the Boltzmann equation to develop a description of the pressure-driven flowrate. Their extended lubrication equation has been used extensively by other researchers to study a variety of problems of practical interest, ranging from air bearings (Alexander et al. 1994) to squeeze film damping in electromechanical devices (Gallis and Torczynski 2004) and has been reviewed extensively (for example, see Cercignani 2006; Szeri 2011). Although the dense-fluid lubrication research community has made significant strides toward treating nanoscale lubrication phenomena (Fillot et al. 2011; Savio et al. 2015, 2016) (as well as other complex physical phenomena, such as cavitation), it appears to have overlooked the GLE approach and its potential. Our objective here is to highlight this potential, demonstrate the feasibility of the approach using an example test problem and finally highlight some of the challenges and open problems unique to the dense-fluid case.

Here, we would be remiss to not discuss the work of Borg et al. (2013), who also proposed a general method for solving multiscale problems of high aspect ratio which would thus be applicable to the lubrication problems discussed here. Their approach is based on the homogeneous multiscale method (HMM) (Ren and Weinan 2005) which aims to minimize the computational cost by using MD simulation only in a fraction of the computational domain. Although clearly related to the approach discussed here, the two approaches are also significantly different. The work by Borg et al. is in principle more general (can be applied to high aspect ratio problems other than of lubrication type), but relies on online MD simulations; in contrast, we believe that a GLE approach would be preferable for treating lubrication problems for a number of reasons. First, beyond developing the closure that specifies the flowrate as a response to the pressure gradient, online MD simulations and numerical approximations [e.g., interpolation between MD domains such as the one used in Borg et al. (2013)] are not required; in fact, this simplicity in some cases enables analytical solutions (as is the case for the validation problem considered here); moreover, the closure could also be obtained from experiments. Second, a GLE can be seamlessly integrated (both from a theoretical and a code development point of view) with other lubrication equation analyses (e.g., matching of solutions in different domains), but even more generally, with other analyses already developed to interface with lubrication equation treatments.

Although a comprehensive review of previous work on models of transport beyond the Navier–Stokes is outside the scope of our work, we would like to briefly discuss some recent findings that are relevant to our MD results discussed in Sect. 3. First we note that a number of recent studies suggest that deviations from the traditional no-slip Navier–Stokes description are due to the presence of additional effects that can be taken into account within the Navier–Stokes constitutive framework, rather than complete failure of the latter (Yoshida and Bocquet 2016; Schlaich et al. 2017; Holland et al. 2015). These effects include (of course) slip, different viscosities in different regions of the physical domain (Schlaich et al. 2017) due to fluid layering (Wang and Hadjiconstantinou 2017), a reduction in the effective domain size due to the gap between the solid and fluid (Yoshida and Bocquet 2016; Ghorbanian et al. 2016) caused by the fluid-solid interaction (Wang and Hadjiconstantinou 2015, 2017), a reduction in the effective fluid density (Ghorbanian et al. 2016) due to fluid layering, and others. On the other hand, it is fair to say that no definite conclusion has been reached yet, since no general agreement exists on what these effects are and whether they are specific to the fluid-solid system under consideration or even the flow geometry. Moreover, some studies find changes to the constitutive relation that are incompatible with the Navier–Stokes description (Travis et al. 1997) or of unclear origin (Ghorbanian and Beskok 2016). As a result, in the context of the Navier–Stokes description we will use the term "failure" (or the related expression "beyond Navier–Stokes") to refer to deviations from the *traditional* macroscale Navier–Stokes description that given the above discussion may not *necessarily* be a result of complete failure of the Navier–Stokes constitutive framework. In fact, as already pointed out before and extensively discussed below, the GLE is an attempt to enable solutions of a particular class of problems (lubrication) without requiring a resolution to the above questions.

The present paper is organized as follows. In the next section (Sect. 2), we briefly review lubrication theory and show how it can be generalized to arbitrary lengthscales. In Sect. 3, we validate the GLE approach using an example lubricant–wall combination and compare the results against full MD simulation. We conclude with Sect. 4, in which we review our results and discuss possible extensions and improvements, as well as more general directions for future work.

2 Extending the Reynolds equation beyond Navier–Stokes

The narrow-gap assumptions that underlie classical lubrication theory (see Leal 2007; Cameron 1983; Szeri 2011 for a detailed description) remain applicable to a large class of

problems even at nanometer-size lengthscales (Gallis and Torczynski 2004; Alexander et al. 1994). We start the development of a lubrication equation valid at those lengthscales by reviewing the main ingredients associated with the classical (Navier–Stokes-based) Reynolds equation.

2.1 Background: the Reynolds equation

Consider an incompressible thin liquid film as shown in Fig. 1. Let x, y, z denote the cartesian coordinates along the $\hat{\mathbf{x}}$, $\hat{\mathbf{y}}$ and $\hat{\mathbf{z}}$ directions, respectively, and u, v, w denote the components of the fluid velocity vector, $\mathbf{u}$, in the same respective directions. As shown in Fig. 1, the film thickness is aligned with the $\hat{\mathbf{y}}$ direction. In the interest of simplicity, we will limit the discussion to flows of the type depicted in the figure, in which no flow exists in the $\hat{\mathbf{z}}$ direction (also $\partial/\partial z = 0$) and only the lower boundary moves in the negative $\hat{\mathbf{x}}$ direction with speed U, while the gap height is characterized by $h = h(x)$.

Let h_0 denote the characteristic film lengthscale in the transverse direction, $\hat{\mathbf{y}}$, and L the characteristic lengthscale in the axial direction $\hat{\mathbf{x}}$. Under the assumption $\varepsilon = h_0/L \ll 1$, the dynamical flow variables can be written in terms of their perturbation expansions in powers of ε; for example, the flow velocity in the axial direction can be expanded as $u = u^0 + \varepsilon u^1 + O(\varepsilon^2)$. Considering only leading order terms and using impermeability constraints at the walls, the continuity equation can be integrated over the film thickness to obtain (Leal 2007)

$$\frac{\partial h}{\partial t} + \frac{\partial Q^0}{\partial x} = 0 \tag{1}$$

where

$$Q^0 = \int_0^{h(x)} u^0 \mathrm{d}y \tag{2}$$

is the (local) volumetric flow rate. The above discussion follows the derivation in Leal (2007); derivation of the Reynolds Equation in the presence of slip at the boundaries is discussed in Burgdorfer (1959).

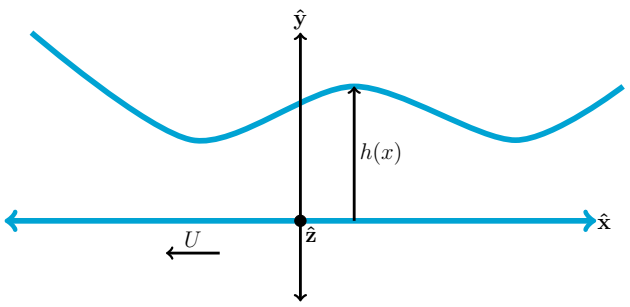

Fig. 1 Sketch of a typical lubrication analysis geometry

The traditional Reynolds lubrication equation

$$\frac{\partial h}{\partial t} = \frac{\partial}{\partial x}\left(\frac{h^3}{12\mu}\frac{\mathrm{d}p^0}{\mathrm{d}x} + \frac{Uh}{2}\right). \tag{3}$$

is obtained through the substitution

$$Q^0 = -\frac{h^3}{12\mu}\frac{\mathrm{d}p^0}{\mathrm{d}x} - \frac{Uh}{2} \tag{4}$$

in (1), where μ denotes the fluid viscosity and p^0 denotes the zeroth-order term in the expansion of the pressure field $p = p^0 + \varepsilon p^1 + O(\varepsilon^2)$, related to u^0 via the Navier–Stokes equation for fully developed—not changing in the flow direction, due to, for example, entrance effects—pressure-driven flow

$$\frac{\mathrm{d}p^0}{\mathrm{d}x} = \mu\frac{\partial^2 u^0}{\partial y^2} \tag{5}$$

In expression (4), rewritten here

$$Q = -\frac{h^3}{12\mu}\frac{\mathrm{d}p}{\mathrm{d}x} - \frac{Uh}{2} \tag{6}$$

without the superscript 0, which will be henceforth omitted in the interest of simplicity, the first term represents the pressure-driven (Poiseuille) component of the flow rate, while the second term represents the flow rate due to the motion of the lower boundary and will be referred to as the Couette component of the flowrate. They will be denoted by Q_P^{NS} and Q_C^{NS}, respectively, where the superscript NS highlights their origin in the Navier–Stokes description (5).

2.2 Generalized lubrication equation

We begin by noting that Eq. (1) is a statement of mass conservation and is thus valid at all lengthscales; the assumption of Navier–Stokes behavior only enters via (6). In other words, if an expression for $Q = Q_P + Q_C$ valid beyond Navier–Stokes can be developed, the resulting lubrication equation will also be valid beyond Navier–Stokes.

We also note that provided the upper and lower bounding surfaces are identical in structure and as far as wall–fluid interactions are concerned, the Couette flowrate remains the same as above, that is, $Q_C = Q_C^{\mathrm{NS}}$; in particular, if $-U\,\hat{\mathbf{x}}$ is the relative velocity between the walls, $Q_C = -Uh/2$.

To introduce a more general form for the pressure-driven component of the flowrate, we argue that it is reasonable to expect that the fluid response *in fully developed flows* is proportional to the pressure gradient and thus can be written in the form

$$Q_P = -\tilde{Q}_P(A, h, \rho, T, B)\frac{\mathrm{d}p}{\mathrm{d}x}, \tag{7}$$

where A denotes the (set of parameters characterizing the) fluid of interest, B denotes the (set of parameters characterizing the) boundary interaction for the particular fluid–wall combination considered, ρ denotes the fluid density and T denotes the temperature. The more general form of the lubrication equation is thus

$$\frac{\partial h}{\partial t} = \frac{\partial}{\partial x}\left(\tilde{Q}_P(A,h,\rho,T,B)\frac{\mathrm{d}p}{\mathrm{d}x} + \frac{Uh}{2}\right) \tag{8}$$

One might expect that $\tilde{Q}_P \sim \mathcal{O}(h^n)$, with $1 \leq n \leq 3$, since $n = 3$ for Navier–Stokes with no-slip (and thus $\tilde{Q}_P \propto h^3$ as $h/\hat{\sigma} \to \infty$), while $n = 1$ appears to be a reasonable lower bound, since the flowrate is expected to be proportional to the channel width. Recalling the dilute gas case (Fukui and Kaneko 1988) is instructive: in this case, the pressure-driven flowrate can be written as

$$Q_P = -h^2\sqrt{2RT}\mathcal{Q}(\mathrm{Kn},B)\frac{\mathrm{d}p}{\mathrm{d}x} \tag{9}$$

where $\mathcal{Q}(\mathrm{Kn},B)$ is a dimensionless coefficient that depends on $\mathrm{Kn} = \lambda/h$, where $\lambda = m/(\sqrt{2}\pi\rho\sigma^2)$ is the mean free path, σ is the hard-sphere diameter, R is the specific gas constant, and B represents the effect of the gas–wall interaction (e.g., via one or more accommodation coefficients) (Cercignani 2006). Therefore, $\tilde{Q}_P(A,h,\rho,T,B) = h^2\sqrt{2RT}\mathcal{Q}(\mathrm{Kn},B)$, where $A = \{m,\sigma\}$.

Unfortunately, $v_m = \sqrt{2RT}$ is unlikely to be an appropriate characteristic molecular velocity for the dense-fluid case. In other words, $\tilde{Q}_P = h^2 v_m \mathcal{Q}(A,h,\rho,T,B)$ is unlikely to correctly scale dense-fluid flowrate data. Despite progress toward developing quantitative models of flow under extreme nanoconfinement (see Schlaich et al. 2017 for an example involving water), in the absence of a general description for the flowrate, $\tilde{Q}$ can be scaled using the traditional macroscopic formulation, namely $\tilde{Q}_P = h^3/(12\mu(\rho,T))F(A,h,\rho,T,B)$, where $F(A,h,\rho,T,B)$ is an *arbitrary* function to be determined by MD simulations or experiments for the fluid of interest and the requirement that $F(A,h,\rho,T,B) \to 1$ as $h/\hat{\sigma} \to \infty$.

We close by noting that although some "empiricism" is required currently, the simplification introduced by the GLE is still considerable: as with any constitutive relation, $\tilde{Q}_P$ need only be determined once, in a fully developed lower-dimensional setting (from a plane Poiseuille flow). Once determined, Eq. (8) can be applied to arbitrary geometries (provided they satisfy the appropriate lubrication approximation criteria).

3 Validation

In this section we validate the ideas discussed in Sect. 2.2 by comparing solutions of the GLE for a particular fluid-solid combination with MD simulations of the same system in a model lubrication geometry. The working fluid in this validation problem is n-hexadecane, while the solid walls are iron. In the following subsection we use MD simulations for determining $\tilde{Q}_P$ for the n-hexadecane-iron fluid–wall system. In Sect. 3.2 we obtain an analytical solution of (8) for the model problem based on the constitutive relation of Sect. 3.1. In Sect. 3.3 we compare MD simulation results with the obtained analytical solution.

3.1 Determining $\tilde{Q}_P$

In order to determine the unknown constitutive relation $\tilde{Q}_P(A,h,\rho,T,B)$ we perform MD simulations in 2-D channels under fully developed conditions for a wide range of h values, namely $1\,\mathrm{nm} \lesssim h \lesssim 11\,\mathrm{nm}$, at a pressure of $p_0 = 80\,\mathrm{MPa}$ and temperature of $T_0 = 450\,\mathrm{K}$. More details on the MD simulations can be found in "Appendix A".

Our validation problem was designed with typical lubrication problems in mind, in which the wall–fluid interaction does not vary as a function of space and thus no variation in B need be considered. Moreover, we note that in typical nanoscale problems flow velocities are sufficiently small to make the isothermal assumption well justified. Given the above, as explained in detail in the "Appendix", care was taken to ensure that our validation problems were also consistent with these assumptions. Specifically, U was sufficiently small for temperature and density variations to be small [the latter due to incompressibility of the dense fluid (Szeri 2011)], justifying the approximation $\tilde{Q}_P(A,h,\rho,T,B) \approx \tilde{Q}_P(A,h,\rho_0,T_0,B_0)$. By verifying that shear rates in all our simulations were sufficiently small for linear response to be valid (see "Appendix"), we can thus expect variations in $\tilde{Q}_P$ to come only from variations in h, that is, we can proceed by taking $\tilde{Q}_P(A_0,h,\rho_0,T_0,B_0) = \tilde{Q}_P(h)$.

One possible form for $\tilde{Q}_P(h)$ follows from using the fact that the flowrate must approach the well-known slip-corrected Poiseuille flowrate for $h/\hat{\sigma} \gg 1$. Specifically, we use the form

$$\tilde{Q}_P = \left(\frac{h^3}{12\mu}\left(1 + \frac{6L_s}{h}\right)\right) \times F(h), \tag{10}$$

where L_s denotes a slip length, while $F(h)$ is responsible for capturing deviations from the slip-corrected Poiseuille flowrate and thus needs to satisfy the requirement $F(h) \to 1$ as $h/\hat{\sigma} \gg 1$. Here it is important to note that the form (10) does not imply an underlying assumption of slip flow, since $F(h)$ is still *arbitrary* (to be determined for each fluid from MD or experimental data). Writing (10) is akin to setting out to describe the dilute gas data with an expression of the form $\tilde{Q}_P = h^3(1 + 6L_S/h)\sqrt{2RT}\mathcal{Q}'/12\mu$, which amounts to the rescaling $\mathcal{Q}' = 12\mu\mathcal{Q}/(h + 6L_S)$. Clearly, the two are

equivalent and do not imply the presence of any restrictions on $\tilde{Q}_P$.

Our MD simulation results for the flowrate are summarized in Fig. 2. Surprisingly, we find that choosing $F = 1\ \forall\ h$ results in a good least-squares fit to the flowrate. In other words, for *the particular system studied here* the constitutive relation for the flowrate is given by

$$\tilde{Q}_P^* = \frac{h^3}{12\mu^*}\left(1 + \frac{6L_s^*}{h}\right). \tag{11}$$

where $\mu^* = 0.67$ mPas and $L_s^* = 3.0$ nm have been determined by a least-squares fit to the MD data shown in the figure.

This finding, namely that the MD flowrates can be described by a slip-corrected Navier–Stokes expression (11) [i.e., that $F = 1$ in (10)] for all h is a rather unexpected and perhaps fortuitous result, likely specific to the fluid-solid system considered here. We note that the values $\mu^* = 0.67$ mPas and $L_s^* = 3.0$ nm, determined from a least-squares fit to all flowrate data ($1.4\,\text{nm} \le h \le 10.8$ nm), are quite different from the viscosity and slip length obtained by fitting the slip-corrected Poiseuille velocity profile to our y-resolved MD data for $h \gtrsim 6$ nm where the slip flow description is expected to be valid.

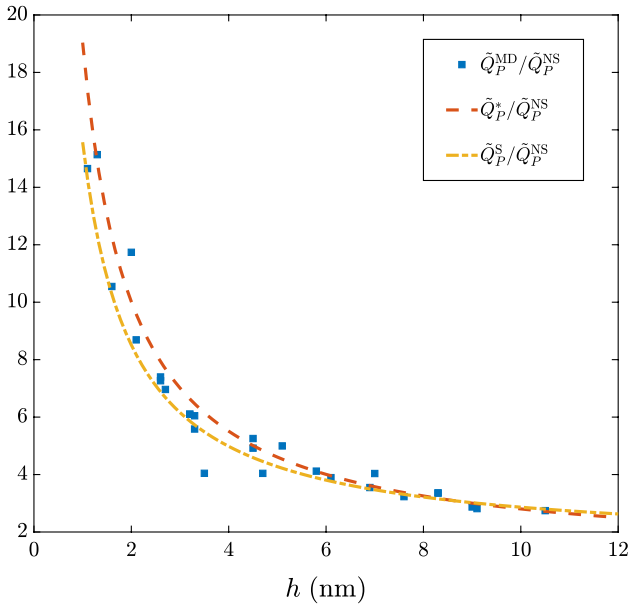

Fig. 2 Flowrates for a range of channel heights $1.4\,\text{nm} \le h \le 10.8$ nm. Comparison between the MD simulation results (denoted by $\tilde{Q}_P^{\mathrm{MD}}$) and expression (11) (denoted by $\tilde{Q}_P^*$). Expression (10) with $F = 1$ and parameters $\mu = \hat{\mu}$ and $L_s = \hat{L}_s$ (slip flow with parameters extracted from large channels) is also shown and is denoted by Q_P^{S}. All results are normalized by $\tilde{Q}_P^{\mathrm{NS}}$ (no-slip Navier–Stokes flowrate)

Selected y-resolved velocity profiles are shown in Fig. 3. This figure shows that the coefficients $\mu^* = 0.67$ mPa s and $L_s^* = 3.0$ nm, are not necessarily able to describe the y-resolved flow profiles in all cases. In particular, we find that for "large" h (specifically, $h \gtrsim 6$ nm), individual y-resolved profiles are well described by a slip-corrected Poiseuille profile with parameters $\hat{\mu} = 0.46$ mPa s and $\hat{L}_s = 1.6$ nm. In the range $3\,\text{nm} \lesssim h \lesssim 6$ nm, although the velocity profiles appear parabolic, the coefficient of viscosity and slip length extracted from fits of y-resolved MD data to slip-corrected Poiseuille profiles are film thickness (h) dependent; this is consistent with previous reports (Ghorbanian and Beskok 2016). For $h \lesssim 3$ nm, the velocity profiles are not parabolic. In other words, $\mu^* = 0.67$ mPa s and $L_s^* = 3$ nm *must be interpreted as parameter values that reproduce the flowrate data* when used in (11) but *do not correspond to viscosity and slip length values in the Navier–Stokes sense*. The relatively small difference between $\tilde{Q}_P^*$ and the slip flowrate $\tilde{Q}_P^{\mathrm{S}}$ (obtained using parameters $\hat{\mu}$ and $\hat{L}_s$) shown in Fig. 2, is also consistent with the findings of Ghorbanian and Beskok (2016) which suggest that the flowrate may exhibit smaller deviations from macroscopic results than other quantities, because as an integral quantity it is more sensitive to cancelation of competing effects.

3.2 The barrel drop problem

Figure 4 shows the "barrel drop" geometry used for validation of the ideas presented in this paper. In this problem, flow occurs due to the motion of the lower wall in the negative $\hat{\mathbf{x}}$ direction with velocity U, as assumed in the lubrication Eq. (8). The upper wall is stationary and of parabolic shape. Thus, the gap height as a function of the axial coordinate is given by $h(x) = h_0 + a(x - L_x/2)^2$, where L_x is the length of the domain in the $\hat{\mathbf{x}}$ direction.

In a general case, equation (8) would have to be solved numerically (say, using a finite volume scheme). In this case, however, the simplicity of the barrel drop geometry and the constitutive relation (10) makes a semi-analytical solution for the pressure distribution possible. Using the fact that $\partial h/\partial t = 0$, we integrate (8) once to obtain the constant volumetric flowrate

$$Q = -\frac{Uh(x)}{2} - \frac{\mathrm{d}p}{\mathrm{d}x}\tilde{Q}_P^*(h(x)) \tag{12}$$

where $\tilde{Q}_P^*(h(x))$ is given in (11). Solving for the pressure, we obtain

$$p(x) = p_0 - \int_0^x \frac{2Q + Uh(x')}{\tilde{Q}_P^*(h(x'))}\,\mathrm{d}x' \tag{13}$$

The flowrate Q can be calculated from the following expression,

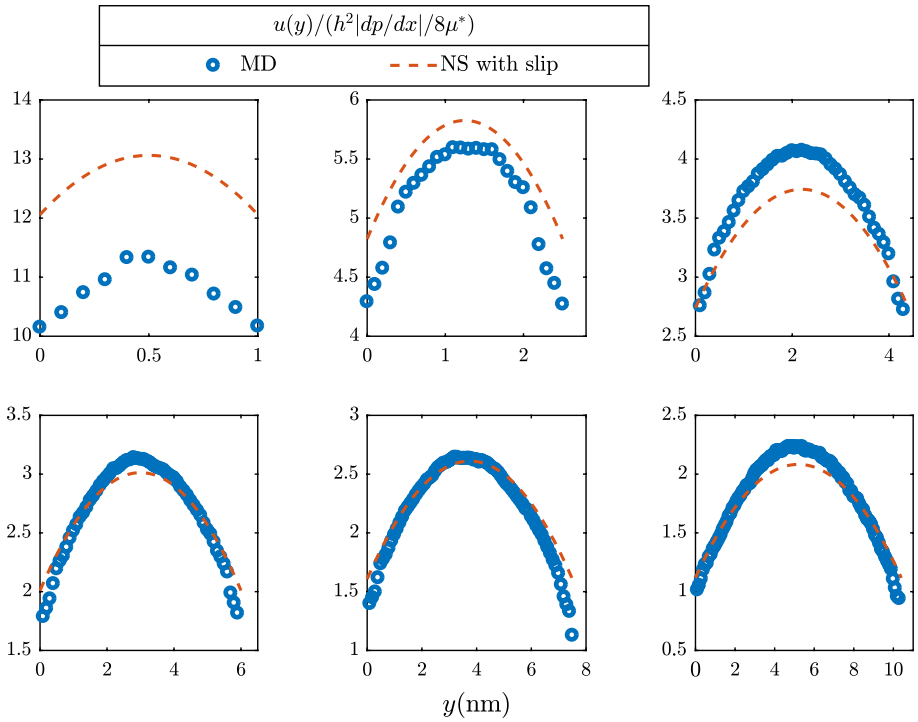

Fig. 3 Normalized velocity profiles for films of different thicknesses in "pressure-driven" flow. Blue circles denote MD simulation data, while the red lines are the velocities predicted by slip-corrected Navier–Stokes with parameters L_s^* and μ^*. The channel widths considered in the order left to right, top to bottom are 1.4, 2.9, 4.8, 6.4, 7.8 and 10.8 nm (color figure online)

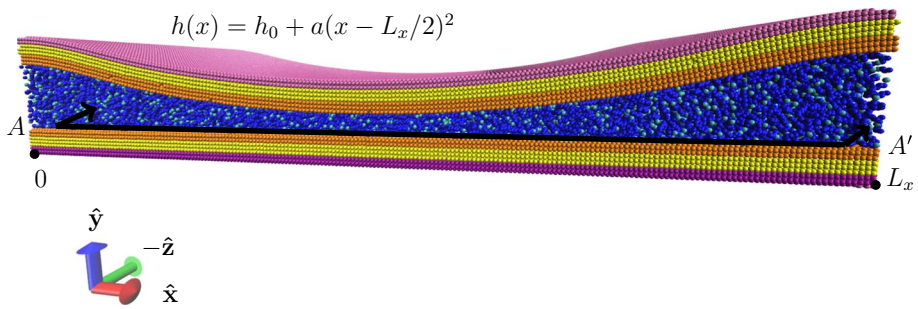

Fig. 4 A schematic model of the "barrel drop" lubrication geometry, which is used in the MD validation problem. L_x is the size of the MD simulation box in the axial direction $\hat{\mathbf{x}}$. The section at A-A' shows the $x-z$ plane along which the pressure is measured using the method of planes (Cheung and Yip 1991) (see "Appendix A.3")

$$Q = -\frac{\int_0^{L_x} Uh(x')[\tilde{Q}_P^*(h(x'))]^{-1}\mathrm{d}x'}{\int_0^{L_x} 2[\tilde{Q}_P^*(h(x'))]^{-1}\mathrm{d}x'} \tag{14}$$

obtained on applying periodic boundary conditions $p(0) = p(L_x)$ on the pressure. The constant p_0 can be calculated from the force balance

$$\int_0^{L_x} p(x)\mathrm{d}x = N \tag{15}$$

where N denotes the total normal force per unit depth (in the z direction) acting on the top surface (assumed given). Due to the symmetry of the film thickness profile about $x = 0$, the above relation reduces to (Chandramoorthy 2016):

$$p_0 L_x = N \tag{16}$$

Finally, the analytical pressure distribution can be obtained from (13), using Q and p_0 from (14) and (16).

3.3 Results

In this section we compare the pressure distribution (13) against the corresponding MD result, denoted by p^{MD}. Two such comparisons are performed here for different minimum gap heights (h_0). The first one is for a minimum gap height $h_0 = 3.8$ nm, while the second one is for $h_0 = 1.6$ nm. In the first comparison, shown in Fig. 5, h_0 is sufficiently large to avoid the presence of solvation and disjoining effects which make direct comparison of the pressure fields difficult. The pressure computed from the MD simulation agrees with the analytical pressure distribution closely. Here we recall that, according to our MD results, for $h \lesssim 6$ nm, y-resolved velocity profiles cannot be described by a fixed (h-independent)

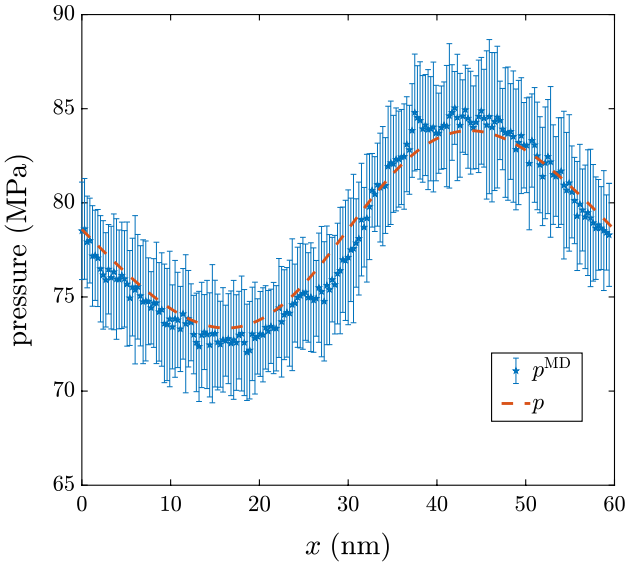

Fig. 5 Comparison between the semi-analytical solution $p(x)$ given by (13) and the pressure computed from the MD simulation, $p^{MD}(x)$, for the "barrel drop" problem with $h_0 = 3.8$ nm

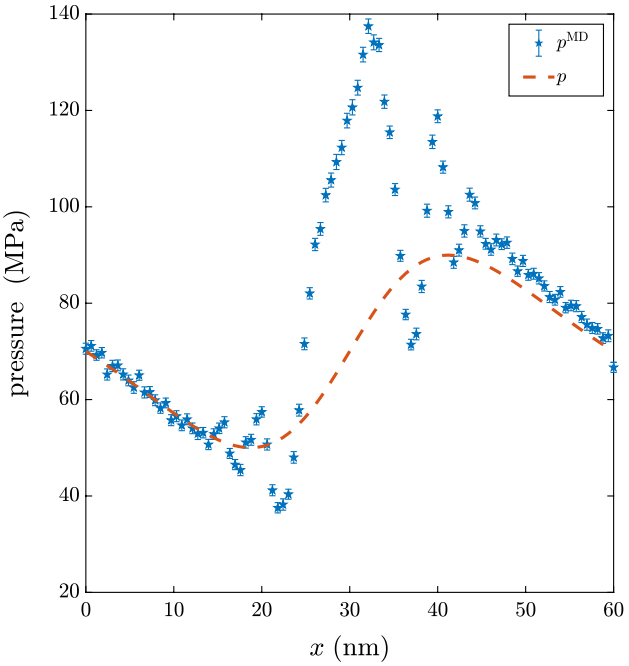

Fig. 6 Comparison between the semi-analytical solution $p(x)$ given by (13) and the pressure computed from the MD simulation, $p^{MD}(x)$, for the "barrel drop" problem with $h_0 = 1.6$ nm As $h \to \hat{\sigma}$, disjoining and solvation effects become important. The latter are particularly apparent

viscosity and slip length, and thus, a lubrication approach based on the traditional Reynolds equation would not be valid.

As stated above, validation at smaller gap heights is complicated by the appearance of solvation (structuring) and disjoining pressure effects (Israelachvili 2011; Kato and Matsuoka 1999). Disjoining pressure effects are caused by long-range (van der Waals) forces and have been considered in a variety of contexts, most notably wetting (de Gennes 1985). Solvation forces result from the entropic contribution of fluid layering at the wall (Israelachvili 2011); as a result, they are important when the characteristic lengthscale h is comparable to the layering thickness, that is, only under extreme confinement (Kato and Matsuoka 1999; Gravelle et al. 2016).

Figure 6 shows p^{MD} for the barrel drop case with $h_0 = 1.6$ nm; although both solvation and disjoining effects are important at this scale, solvation effects are particularly evident in the regions corresponding to $h \lesssim 3$ nm due to their distinctive oscillatory nature.

Solvation and disjoining pressure effects can be included in the proposed formulation by solving Eq. (8) subject to the boundary conditions $p(0) = p(L_x)$ and

$$N = \int_0^{L_x} [p(x) + p_s(h(x)) + p_d(h(x))]\, \mathrm{d}x \tag{17}$$

where $p_s(h(x))$ denotes the solvation pressure and

$$p_d(h(x)) = \frac{A_H}{6\pi h^3(x)} \tag{18}$$

is the disjoining pressure, where A_H denotes the Hamaker constant (Israelachvili 2011).

It is important to note that although p_s and p_d are of $O(\epsilon^0)$, they are not included in the GLE (8) because, as discussed in Sect. 2.1, the (local) flowrate Q is calculated from the response to the zeroth-order balance (5), while

$$\frac{\mathrm{d}}{\mathrm{d}x}(p_d + p_s) = \frac{\mathrm{d}(p_s + p_d)}{\mathrm{d}h}\frac{\mathrm{d}h}{\mathrm{d}x} \tag{19}$$

is of order ϵ^1.

Although the molecular origin of the solvation pressure is well understood (Israelachvili 2011; Henderson 1986), reliable expressions for predicting its magnitude for various fluids are not available. However, Gravelle et al. (2016) have recently shown that an expression of the form

$$p_s^{2D}(h(x)) = -\rho_\infty k_B T \cos(2\pi h(x)/\delta) \exp(-h(x)/\delta). \tag{20}$$

developed for a hard-sphere fluid in two dimensions, can be used to describe this effect in water, provided ρ_∞, originally defined as the bulk fluid density far from the wall, was treated as an adjustable parameter. In the above expression, δ is a parameter related to the fluid structure and is thus expected to be of order $\hat{\sigma}$. We use p_s^{2D} above to model p_s, with the value of δ and ρ_∞ determined from our simulation data. To determine δ we use the Fourier transform of $p^{MD} - p$, shown in Fig. 7, which exhibits a single peak at

0.4 nm, confirming the sinusoidal dependence of p_s on h and suggesting $\delta = 0.4$ nm. This value is known from surface force measurements and MD simulations (Ribarsky and Landman 1992; Christenson et al. 1987) to be close to the thickness of a layer of n-hexadecane confined between crystalline substrates.

Using this value for δ and treating ρ_∞ and A_H as adjustable (fitting) constants, we show in Fig. 8 that the decomposition $p + p_s + p_d$ can model p^{MD} for h as low as 1.6 nm.

4 Discussion and conclusions

We have discussed a generalized lubrication equation framework for the solution of dense-fluid lubrication problems at the nanometer scale. The framework is based on the observation that under the lubrication approximation, the closure required is significantly less difficult to obtain than for the general flow case.

In the example considered here, it was assumed that the two solid surfaces interact with the fluid identically and thus the Couette component of the flowrate, by symmetry, remains equal to its Navier–Stokes no-slip value. The proposed methodology can be extended to cases where interactions are asymmetric by developing a constitutive relation for the Couette component of the flowrate. Although in the example lubricant–wall model studied here the flowrate was reproduced using a slip flow-based relationship, the GLE is in no way reliant on the validity of a slip flow description. As an example, see the dilute gas case (Eq. (9)) and the related discussion in Sect. 2.2. Developing a *general* scaling relation for $\tilde{Q}_P$ in terms of the governing molecular parameters for dense fluids is the subject of future work, although significant progress has been made for particular fluid-solid systems (see Sect. 1). Such a relation would potentially reduce the number of simulations/experiments required to describe $\tilde{Q}_P(A, h, \rho, T, B)$ for a particular fluid.

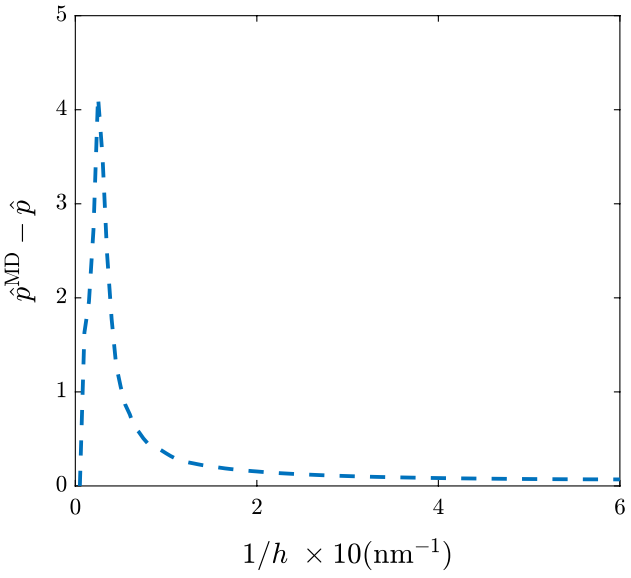

Fig. 7 The Fourier transform of $p^{\mathrm{MD}} - p$ clearly shows a peak at $1/h = 2.5$ (corresponding to 0.4 nm), indicating the dominant wavelength associated with the spatial variation of solvation effects

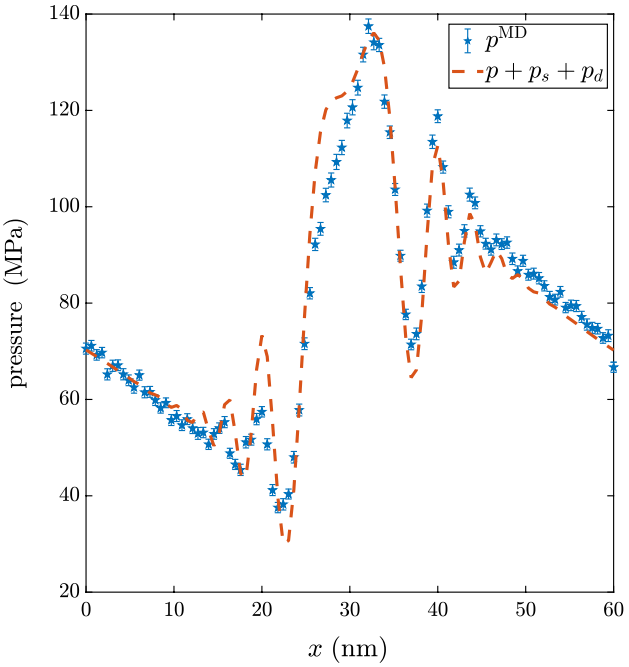

Fig. 8 Comparison between $p(x) + p_s(h(x)) + p_d(h(x))$, given by (13) and (20), respectively, and the pressure computed from the MD simulation, $p^{\mathrm{MD}}(x)$, for the "barrel drop" problem with $h_0 = 1.6$ nm

Developing a constitutive relation and solving the resulting GLE is considerably more tractable than brute-force MD simulations for *problems of practical interest*. In fact, the latter is usually impossible, both because of the cost associated with the number of particles required for such simulations, but also because the characteristic timescales of such systems are much longer. For example, the cost associated with the GLE (primarily MD simulations for constructing the constitutive relation) is smaller than the cost of one barrel drop simulation, even though the latter is at lengthscales much smaller than actual problems of practical interest (deliberately chosen for validation purposes, to ensure that an MD solution was feasible). Once the constitutive relation is developed, additional solutions of the GLE come at a cost that is essentially negligible (compared to MD simulations).

For very small film heights, solvation and disjoining effects become important. Fortunately, as in previous work (Gravelle et al. 2016; Kato and Matsuoka 1999), it was shown that these effects can be satisfactorily accounted for by linearly superposing their contribution to the hydrodynamic pressure, requiring minimal modification of the

lubrication equation. Although in both cases (present and previous work Gravelle et al. 2016) good agreement with MD simulations was found by fitting the result for hard spheres in two dimensions, it is clear that our ability to model solvation effects for more realistic fluids is very limited and needs to be improved.

Acknowledgements The authors would like to thank Mathew Swisher and Gerald J. Wang for help with the computations and many helpful comments and suggestions during the course of this research. This work was sponsored by the Consortium on Lubrication in Internal Combustion Engines with additional support from Argonne National Laboratory and the US Department of Energy. The current consortium members are Daimler, Mahle, MTU Friedrichshafen, PSA Peugeot Citroën, Renault, Shell, Toyota, Volkswagen, Volvo Cars, Volvo Trucks and Weichai Power. The use of the Center for Nanoscale Materials, an Office of Science user facility, was supported by the U. S. Department of Energy, Office of Science, Office of Basic Energy Sciences, under Contract No. DE-AC02-06CH11357.

Appendix A. MD simulations

All MD simulations in this work were performed using the software package LAMMPS (Plimpton 1995).

As explained in Sect. 2.2, the constitutive relation was developed by studying fully developed flow in two-dimensional channels. The validation was performed in the barrel drop geometry of Fig. 4, which is a significantly larger-scale problem. In both cases, the model lubricant is *n*-hexadecane, simulated using the TraPPE potential (Martin and Siepmann 1999), while the system solid boundaries are atomically smooth iron (BCC Fe) walls, simulated using the Embedded Atom Method—Finnis Sinclair (Mendelev 2010; Mendelev et al. 2003; Ackland et al. 1997) potential. The Lennard-Jones (LJ) parameters used between well-separated pseudo-atoms, i.e, a pair of pseudo-atoms separated by three or more pseudo-atoms within the same molecule or a pair belonging to two different molecules within the fluid, are given in Table 1. The LJ parameters of interaction between atoms of unlike types were calculated using the Lorentz–Berthelot mixing rules.

Bond stretching in the fluid molecules was modeled via a harmonic potential of the form, $U_{ij} = \frac{k_r}{2}(r_{ij} - r_0)^2$, where $r_0 = 1.54$ Å is the equilibrium bond length and k_r, the bond stretching parameter taken here to have the value 19.5139 eV/Å^2 (chosen from Lòpez-Lemus et al. 2006). The bending energy associated with variations of the angle between 3 adjacent atoms connected through bonds was modeled through a harmonic potential (Martin and Siepmann 1999) of the form $U_{\text{bend}} = \frac{k_\theta}{2}(\theta - \theta_0)^2$, where the bending parameter k_θ is taken as 2.6925 eV and the equilibrium angle, $\theta_0 = 114°$. The torsional potential that arises due to the bending of the dihedral angle, ϕ, was given by an OPLS style potential (Watkins and Jorgensen 2001):

$$U_{\text{torsion}} = \frac{c_1}{2}(1 + \cos\phi) + \frac{c_2}{2}(1 - \cos(2\phi)) + \frac{c_3}{2}(1 + \cos(3\phi))$$

The parameters were taken from Martin and Siepmann (1999) to be:

$$c_1 = 0.05774 \quad c_2 = -0.0117524, \quad c_3 = 0.136382$$

The interactions between the solid and the liquid atoms were modeled using the LJ potential. The parameters for the wall–fluid interaction potential were computed through the Lorentz–Berthelot mixing rules, using the self-interaction parameters listed in Table 1. Note that the self-interaction parameters for Fe were taken from Berro et al. (2010) (developed for more realistic simulation of Fe oxide surfaces) and are different from those reported in the literature for BCC Fe (see Zhen and Davies (1983), for example).

Table 1 The LJ parameters of interaction between different atomic species used in the paper

Type of pseudo-atom *i*	Type of pseudo-atom *j*	σ (Å)	ϵ (eV)
CH_2	CH_2	3.95	0.003964
CH_3	CH_3	3.75	0.008445
CH_3	CH_2	3.85	0.0058
Fe	Fe	2.2	0.02947

Appendix A.1. Channel flow

The simulations were performed in channels of length 99.94 Å in the flow direction, $\hat{\mathbf{x}}$, and width 71.38 Å, in the $\hat{\mathbf{z}}$ direction. The channel width in the transverse $\hat{\mathbf{y}}$ direction, denoted by h, varied between 1.4 and 10.8 nm. Fluid motion was generated by applying a body force per unit mass in the flow direction, g, while periodic boundary conditions were imposed in the flow direction, $\hat{\mathbf{x}}$, thus eliminating entrance effects and making the flow fully developed by construction. Periodic boundary conditions were also applied in the homogeneous (depth) direction, $\hat{\mathbf{z}}$. In the transverse, $\hat{\mathbf{y}}$, direction, the fluid was bounded by two solid walls. Each wall consisted of eight layers of atomically smooth BCC Fe (001) surface, of thickness 22.84 Å. The two layers furthest away from the fluid were frozen (using `LAMMPS`'s `fix rigid`) and provided the wall structure; the adjacent three layers of atoms were responsible for maintaining the simulation temperature at 450 K and were thus thermostatted using a Nosé–Hoover thermostat. No constraints were imposed on the three layers closest to the liquid. The fluid pressure was maintained at 80 MPa, by applying a normal force to the frozen solid layers. To avoid thermostat-induced artifacts (Pahlavan and Freund 2011), no thermostat was applied

to the fluid molecules during the data sampling phase. (A Langevin thermostat was used for the initial equilibration phase.) Viscous heat generated within the fluid was removed by the thermostatted wall molecules. To ensure small temperature variations, the maximum fluid velocity was on the order of 50 m/s or less, resulting in a maximum temperature variation of $O(5\ \mathrm{K})$, which is sufficiently small for the isothermal assumption to be valid. We have determined empirically that taking the body force to be sufficiently small so that temperature variations were small (and thus, nonlinearities due to temperature-dependent transport coefficients were negligible) also ensured linear response, for which pressure-driven and body force-driven flow are expected to be equivalent. This equivalence was validated by our results of Sect. 3.1. We also note that actual flow speeds encountered in nanoscale flows are much smaller (usually by many orders of magnitude) than the flow velocities used here [which are large in order to improve signal to noise ratio (Hadjiconstantinou et al. 2003)]; in other words, isothermal flow and linear response assumptions are even more justified for real flows.

Simulation results are shown in Figs. 2 and 3 and discussed in Sect. 3.1. In Fig. 3, $|\mathrm{d}p/\mathrm{d}x|$ represents the "effective pressure gradient magnitude" ($= \rho g$).

Appendix A.2. Barrel drop

The geometry of the barrel drop profile is shown in Fig. 4. Fluid flow was generated by the motion of the lower solid boundary at a speed of $U = 60$ m/s. Both the upper parabolic surface and the lower plane surface consisted of rigid, thermostat and deformable layers, with constraints (including thermostating) analogous to those discussed in the previous section on channel flow. Specifically, heat was removed from the system by thermostating the three wall layers furthest away from the fluid in each wall, and no thermostat was applied to the fluid during the data sampling phase. The extent of the simulation box in the two lateral directions, $\hat{\mathbf{x}}$ and $\hat{\mathbf{z}}$, was $L_x = 59.9$ nm and $L_z = 25.6$ nm, respectively. Based on a characteristic lengthscale $L_c = 40$ nm, the non-dimensional value of the curvature parameter is $aL_c^2/h_0 = 1.845$.

Appendix A.3. Computation of pressure in MD simulations

As is well known from previous work (Cheung and Yip 1991; Todd et al. 1995; Cleri 2001), the Irving–Kirkwood (IK) formula for the stress tensor in a fluid exhibits spurious oscillations near hard system boundaries such as solid walls. As a result, in the present work the fluid pressure is measured by calculating the p_{yy} component of the configurational part of the stress tensor, as the sum of all molecular forces acting across a flat (imaginary) dividing plane whose normal is in the $\hat{\mathbf{y}}$ direction. Specifically, we are using an approach known as the method of planes (MOP) (Todd et al. 1995), in which the configurational part of the stress tensor at location y is calculated by

$$p^c_{yy}(y) = \frac{1}{4L_xL_z}\sum_{ij} F^y_{ij}\Big(\mathrm{sgn}(y_i - y) - \mathrm{sgn}(y_j - y)\Big) \qquad \text{(A.1)}$$

where y_i and y_j are the components of the position vectors of atoms i and j in the $\hat{\mathbf{y}}$ direction at time t, respectively, and F^y_{ij} represents the $\hat{\mathbf{y}}$-component of the force on atom i due to atom j. The force component F^y_{ij} contributes to the configurational pressure only if it acts across the plane at y. The pressure is then given by $p = p_{yy}$; we have independently verified, via simulations in 2D channels that the stress tensor remains isotropic even at these small scales. The above definition assumes pairwise forces between contributing atoms. Stress tensor definitions for systems of particles interacting through many-body forces have only been developed for the virial IK-based formulation (Thompson et al. 2009). To overcome this limitation, here we use the fact that, in the lubrication approximation, the fluid pressure is independent of y. We have thus placed the sampling plane in the narrow gap between wall and liquid, which ensures that any pair of contributing atoms is never both solid or liquid. An additional benefit associated with this choice is that no atom crossings occur across this sampling plane, meaning that the kinetic term

$$p^k_{yy}(y) = \frac{1}{2L_xL_z}\sum_i m_i v_i \frac{d}{dt}\mathrm{sgn}(y_i - y). \qquad \text{(A.2)}$$

does not contribute. In the above equation, m_i is the mass of particle i and v_i is the component of the particle velocity of particle i in the $\hat{\mathbf{y}}$ direction at time t.

Although derived for infinitely large planes, in the case of the barrel drop geometry, in order to resolve the pressure variation in the flow direction, we have applied expression (A.1) locally, that is, over bins of finite extent in the flow ($\hat{\mathbf{x}}$) direction. The number of bins was chosen to balance the need for good axial resolution of the pressure with the need for the number of bins to be as small as possible so that the change in pressure across consecutive bins is small. Specifically, we used 100 bins, with each bin spanning 0.6 nm in the $\hat{\mathbf{x}}$ direction and the size of the periodic box, 25.6 nm, in the $\hat{\mathbf{z}}$ direction.

References

Ackland GJ, Bacon DJ, Calder AF, Harry T (1997) Computer simulation of point defect properties in dilute Fe–Cu alloy using a many-body interatomic potential. Philos Mag A 75:713–732

Alexander FJ, Garcia AL, Alder BJ (1994) Direct simulation Monte Carlo for thin-film bearings. Phys Fluids 6:3854–3860
Allen MP, Tildesley DJ (1989) Computer simulation of liquids. Oxford university press, Oxford
Berro H, Fillot N, Vergne P (2010) Molecular dynamics simulation of surface energy and ZDDP effects on friction in nano-scale lubricated contacts. Tribol Int 43:1811–1822
Borg MK, Lockerby DA, Reese JM (2013) A multiscale method for micro/nano flows of high aspect ratio. J Comput Phys 233:400–413
Burgdorfer A (1959) The influence of the molecular mean free path on the performance of hydrodynamic gas lubricated bearings. ASME J Basic Eng 81:94–100
Cameron A (1983) Basic lubrication theory. Ellis Horwood Ltd., Chichester
Cercignani C (2006) Slow rarefied flows: theory and application to micro-electro-mechanical systems, vol 41. Springer, Berlin
Chandramoorthy N (2016) Molecular dynamics-based approaches for mesoscale lubrication. Master's thesis, Massachusetts Institute of Technology
Cheung KS, Yip S (1991) Atomic-level stress in an inhomogeneous system. J Appl Phys 70:5688–5690
Christenson H, Gruen D, Horn R, Israelachvili J (1987) Structuring in liquid alkanes between solid surfaces: force measurements and mean-field theory. J Chem Phys 87:1834–1841
Cleri F (2001) Representation of mechanical loads in molecular dynamics simulations. Phys Rev B 65:014107
de Gennes P-G (1985) Wetting: statics and dynamics. Rev Mod Phys 57:827
Fillot N, Berro H, Vergne P (2011) From continuous to molecular scale in modelling elastohydrodynamic lubrication: nanoscale surface slip effects on film thickness and friction. Tribol Lett 43:257–266
Frenkel D, Smit B (2002) Understanding molecular simulation: from algorithms to applications, vol 1. Elsevier (formerly published by Academic Press), Amsterdam
Fukui S, Kaneko R (1988) Analysis of ultra-thin gas film lubrication based on linearized Boltzmann equation: first report- derivation of a generalized lubrication equation including thermal creep flow. J Tribol 110:253–261
Gallis MA, Torczynski JR (2004) An improved Reynolds-equation model for gas damping of microbeam motion. J Microelectromech Syst 13:653–659
Ghorbanian J, Beskok A (2016) Scale effects in nano-channel liquid flows. Microfluidics Nanofluidics 20:121
Ghorbanian J, Celebi AT, Beskok A (2016) A phenomenological continuum model for force-driven nano-channel liquid flows. J Chem Phys 145:184109
Gravelle S, Ybert C, Bocquet L, Joly L (2016) Anomalous capillary filling and wettability reversal in nanochannels. Phys Rev E 93:033123
Guo S, Meshot ER, Kuykendall T, Cabrini S, Fornasiero F (2015) Nanofluidic transport through isolated carbon nanotube channels: advances, controversies, and challenges. Adv Mater 27:5726–5737
Hadjiconstantinou NG (2006) The limits of Navier–Stokes theory and kinetic extensions for describing small-scale gaseous hydrodynamics. Phys Fluids 18:111301
Hadjiconstantinou NG, Garcia AL, Bazant MZ, He G (2003) Statistical error in particle simulations of hydrodynamic phenomena. J Comput Phys 187:274–297
Henderson J (1986) Compressibility route to solvation structure. Mol Phys 59:89–96
Holland DM, Lockerby DA, Borg MK, Nicholls WD, Reese JM (2015) Molecular dynamics pre-simulations for nanoscale computational fluid dynamics. Microfluidics Nanofluidics 18:461–474
Israelachvili J (2011) Intermolecular and surface forces. Elsevier, Amsterdam
Kato T, Matsuoka H (1999) Molecular layering in thin-film elastohydrodynamics. Proc Inst Mech Eng Part J J Eng Tribol 213:363–370
Landman U, Luedtke WD, Gao J (1996) Atomic-scale issues in tribology: interfacial junctions and nano-elastohydrodynamics. Langmuir 12:4514–4528
Leal L G (2007) Advanced transport phenomena: fluid mechanics and convective transport processes. Cambridge University Press, Cambridge
Lòpez-Lemus J, Romero-Bastida M, Darden TA, Alejandre J (2006) Liquid-vapour equilibrium of n-alkanes using interface simulations. Mol Phys 104:2413–2421
Martin MG, Siepmann JI (1999) Novel configurational-bias Monte Carlo method for branched molecules. Transferable potentials for phase equilibria. 2. United-atom description of branched alkanes. J Phys Chem B 103:4508–4517
Mattia D, Leese H, Lee KP (2015) Carbon nanotube membranes: from flow enhancement to permeability. J Membr Sci 475:266–272
Mendelev MI et al (2010) Interatomic potentials repository project. http://www.ctcms.nist.gov/potentials/Download/Fe-MIM2/Fe_2.eam.fs. Updated 22 Dec 2010
Mendelev MI, Han S, Srolovitz DJ, Ackland GJ, Sun DY (2003) Development of new interatomic potentials appropriate for crystalline and liquid Iron. Philos Mag 83:3977–3994
Pahlavan AA, Freund JB (2011) Effect of solid properties on slip at a fluid-solid interface. Phys Rev E 83:021602
Plimpton S (1995) Fast parallel algorithms for short-range molecular dynamics. J Comput Phys 117:1–19
Popadić A, Walther JH, Koumoutsakos P, Praprotnik M (2014) Continuum simulations of water flow in carbon nanotube membranes. New J Phys 16:082001
Priezjev NV, Darhuber AA, Troian SM (2005) Slip behavior in liquid films on surfaces of patterned wettability: comparison between continuum and molecular dynamics simulations. Phys Rev E 71:041608
Ren W, Weinan E (2005) Heterogeneous multiscale method for the modeling of complex fluids and micro-fluidics. J Comput Phys 204:1–26
Ribarsky MW, Landman U (1992) Structure and dynamics of n-alkanes confined by solid surfaces. i. stationary crystalline boundaries. J Chem Phys 97:1937–1949
Savio D, Fillot N, Vergne P (2013) A molecular dynamics study of the transition from ultra-thin film lubrication toward local film breakdown. Tribol Lett 50:207–220
Savio D, Fillot N, Vergne P, Hetzler H, Seemann W, Espejel GM (2015) A multiscale study on the wall slip effect in a ceramic-steel contact with nanometer-thick lubricant film by a nano-to-elastohydrodynamic lubrication approach. J Tribol 137:031502
Savio D, Pastewka L, Gumbsch P (2016) Boundary lubrication of heterogeneous surfaces and the onset of cavitation in frictional contacts. Sci Adv 2:e1501585
Schlaich A, Kappler J, Netz RR (2017) Hydration friction in nanoconfinement: from bulk via interfacial to dry friction. Nano Lett 17:5969–5976
Secchi E, Marbach S, Niguès A, Stein D, Siria A, Bocquet L (2016) Massive radius-dependent flow slippage in carbon nanotubes. Nature 537:210–213
Sofos F, Karakasidis T, Liakopoulos A (2009) Transport properties of liquid argon in krypton nanochannels: anisotropy and non-homogeneity introduced by the solid walls. Int J Heat Mass Transf 52:735–743
Szeri AZ (2011) Fluid film lubrication. Cambridge University Press, Cambridge
Thompson AP, Plimpton SJ, Mattson W (2009) General formulation of pressure and stress tensor for arbitrary many-body interaction

potentials under periodic boundary conditions. J Chem Phys 131:154107
Todd B, Evans DJ, Daivis PJ (1995) Pressure tensor for inhomogeneous fluids. Phys Rev E 52:1627
Travis KP, Todd BD, Evans DJ (1997) Departure from Navier–Stokes hydrodynamics in confined fluids. Phys Rev E 55:4288–4295
Wang GJ, Hadjiconstantinou NG (2015) Why are fluid densities so low in carbon nanotubes? Phys Fluids 27:052006
Wang GJ, Hadjiconstantinou NG (2017) Molecular mechanics and structure of the fluid-solid interface in simple fluids. Phys Rev Fluids 2:094201
Watkins EK, Jorgensen WL (2001) Perfluoroalkanes: conformational analysis and liquid-state properties from ab initio and Monte Carlo calculations. J Phys Chem A 105:4118–4125
Yoshida H, Bocquet L (2016) Labyrinthine water flow across multilayer graphene-based membranes: molecular dynamics versus continuum predictions. J Chem Phys 144:234701
Zhen S, Davies GJ (1983) Calculation of the Lennard-Jones n-m potential energy parameters for metals. Physica Status Solidi (a) 78:595–605
Zheng X, Zhu H, Tieu AK, Kosasih B (2005) A molecular dynamics simulation of 3D rough lubricated contact. Tribol Int 67:217–221
Zheng X, Zhu H, Kosasih B, Tieu AK (2013) A molecular dynamics simulation of boundary lubrication of n-alkanes chain length and normal load. Wear 301:62–69